Institute of Physics Publishing | Smart Materials and Structures
Smart Mater. Struct. **15** (2006) 924–930 doi:10.1088/0964-1726/15/4/004

Microscale position control of an electroactive polymer using an anti-windup scheme

Kwansoo Yun and Won-jong Kim[1]

Department of Mechanical Engineering, Texas A&M University, College Station, TX 77843-3123, USA

E-mail: wjkim@tamu.edu

Received 12 October 2004, in final form 23 March 2006
Published 31 May 2006
Online at stacks.iop.org/SMS/15/924

Abstract
Smart materials have been widely used for control actuation. In this paper, we present a microscale position control system using a novel electroactive polymer (EAP). We built a third-order model based on the system identification of the EAP actuator with an autoregressive moving average with exogenous input (ARMAX) method using a chirp signal input from 0.01 Hz to 1 Hz with the magnitude limited to ±7 V. With the derived plant model, we designed a digital PID (proportional–integral–derivative) controller with an integrator anti-windup scheme. We provide test results on macro (0.8 mm) and micro (50 μm) step responses of the EAP actuator, and its position tracking capability is demonstrated. The overshoot decreased from 79.7% to 37.1% and the control effort decreased by 16.3%. The settling time decreased from 1.79 s to 1.61 s. The controller with the anti-windup scheme effectively reduced the degradation in the system performance due to actuator saturation. EAP microgrippers based on the control scheme presented in this paper will have significant applications including picking-and-placing micro-sized objects or as medical instruments.

(Some figures in this article are in colour only in the electronic version)

1. Introduction

Smart materials exhibit physical responses, such as mechanical deformation and heat generation in the presence of applied stimuli, such as electricity, heat, chemical reaction, and pressure. These responses can be used in converting the applied energy into a desired form. The EAP is a class of materials composed of polymers, metals, and other elements that show unique properties. (1) This composite material produces a mechanical motion in response to applied electrical voltage. (2) Conversely, EAP can be used as a sensor by measuring the output voltage generated by imposed mechanical deformation. These properties can be useful in a variety of applications requiring actuation or sensing.

During the last decade, Sadeghipour *et al*, Shahinpoor, Oguru *et al* and Tadokoro *et al* investigated the bending characteristics of ionic polymer metal composite (IPMC) [1–4]. Bar-Cohen *et al* characterized the electromechanical properties of IPMC [5]. An empirical model by Kanno *et al* was developed and optimized with curve-fit routines on open-loop step responses incorporating three stages in the actuator model, i.e., electrical, stress-generation, and mechanical stages [6–8]. Feedback compensators were designed using a similar model in a cantilever configuration to study its open-loop and closed-loop behaviors [9, 10].

Many ionic polymers including IPMC or EAP can be classified as viscoelastic materials, so researchers adopted the Golla–Hughes–McTavish (GHM) method [11]. It enabled the modeling of linear viscoelastic materials using the Young's modulus as a function of frequency [11, 12]. Alvarez and Shahinpoor showed the static and dynamic deflection with the nonlinear equation for large-angle deflections in an elastic cantilever beam by simulation [12]. Prevailing approaches to controller design presume that an applicable model for

[1] Author to whom any correspondence should be addressed.

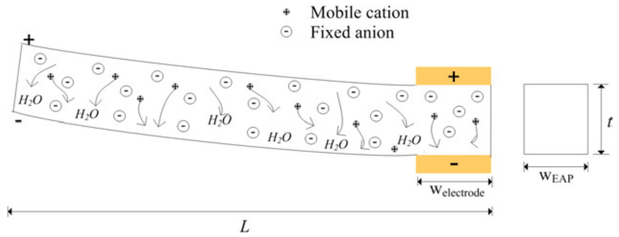

Figure 1. Redistributed charges in an EAP strip caused by the external electric field.

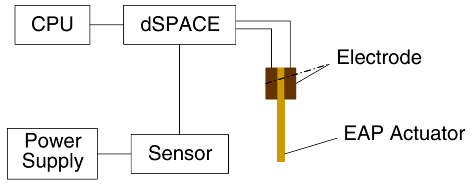

Figure 2. Schematic diagram of the experimental setup.

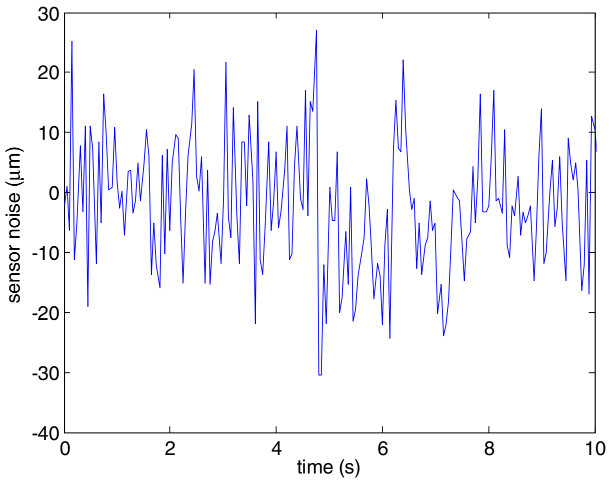

Figure 3. Laser displacement sensor noise profile.

the plant to be controlled is available. Although most real-world dynamic systems are nonlinear, they could usually be approximated in their normal ranges of operation, and relatively simple, lumped-parameter input–output linearized models can often be used. Some EAP materials are now commercially available [13], but their material properties are still under investigation with analytical and numerical approaches.

The step response, as a means for modeling, of EAP was observed to be non-repeatable because its stiffness is a function of the hydration level of the polymer, which might change with respect to time while in continual use. Damping of the ionic polymer actuator in air is much lower than that in water. Thus, feedback control is necessary to decrease the response time of an EAP actuator to a step change in the applied electric field and to reduce overshoot. The position control of the EAP was investigated by using a linear quadratic regulator (LQR) [11, 14], a PID controller with impedance control [15], and a lead-lag compensator [9, 10]. Advanced control algorithms must be developed for EAP or IPMC to compensate for their highly nonlinear and non-repeatable open-loop behaviors.

In this paper, precision position control is demonstrated for an EAP actuator by implementing a digital PID controller with an integrator anti-windup scheme that reduces the performance degradation due to actuator saturation. Section 2 provides an overview of the EAP actuator we developed. Section 3 presents the system identification of its plant model. Section 4 describes the design of the microscale position controller and the anti-windup scheme. In section 5, simulated and experimental results with the closed-loop position control implemented on the EAP actuator are presented.

2. Working principle of an EAP actuator and experimental setup

When an electric field is imposed across an EAP strip, mobile cations freely migrate towards the cathode with water molecules, causing contraction in the positive electrode side. In the meantime, fixed anions towards the anode cause expansion in the negative electrode side [16]. The total charge redistribution inside an EAP-strip actuator in response to the external electric field causes the bending motion and is depicted in figure 1.

An EAP strip is lightweight and highly flexible. It consumes very little power to produce large deformation. It can also operate in wet environments. If EAP is used as a sensor, large displacement by mechanical bending can be measured by sensing the output voltage [16]. Since EAP is used as an ionic actuator/sensor, it would require a solvent medium such as deionized water to operate optimally. If encapsulated using a hydrophobic thin membrane, it can be used in a dry environment for extended operation. The parameters for the experimental EAP strip and the material properties of EAP [13] are provided in table 1.

Table 1. Parameters of the EAP strip used in this research.

Length, L	25.18 mm
Width, w_{eap}	4.24 mm
Thickness, t	0.18 mm
Mass	0.047 g
Density	2.446 g cm^{-3}
Electrode width, w_{el}	14.95 mm
Voltage range	0.1–7.0 V_{rms}
Bending	100% of effective length up to $\pm 90°$
Young's modulus	600 MPa
Strain energy density	15–20 J kg^{-1}

Figure 2 shows a schematic diagram of the experimental setup. Figure 3 shows a noise profile of the laser displacement sensor (Model OADM 20I44/404790) with a resolution of 5 μm and a standard deviation of 10 μm from Baumer Electric measuring the tip displacement of the EAP actuator. This position measurement is fed to a 16-bit analogue-to-digital (A/D) converter channel of a DS1102 floating-point digital-signal-processing (DSP) board from dSPACE. This DSP board communicates with a Pentium III personal computer for user interface. The control voltage to actuate the EAP strip is generated through a 16-bit digital-to-analogue (D/A) converter channel of the DSP board.

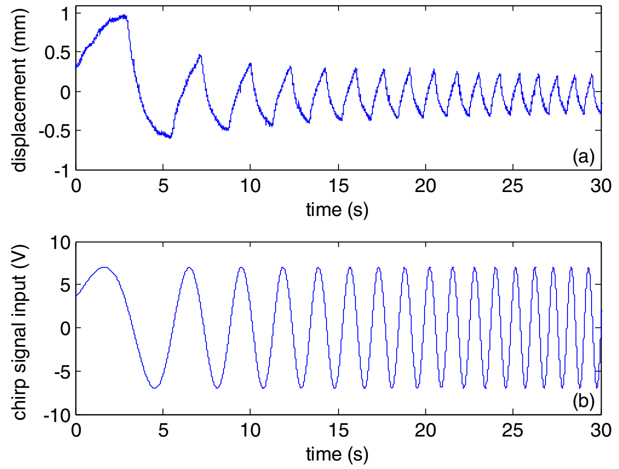

Figure 4. (a) The open-loop response of the EAP strip to (b) a linear swept-frequency (chirp) signal. At $t = 0$, the frequency was 0.01 Hz and continuously increased to 1 Hz at $t = 30$ s.

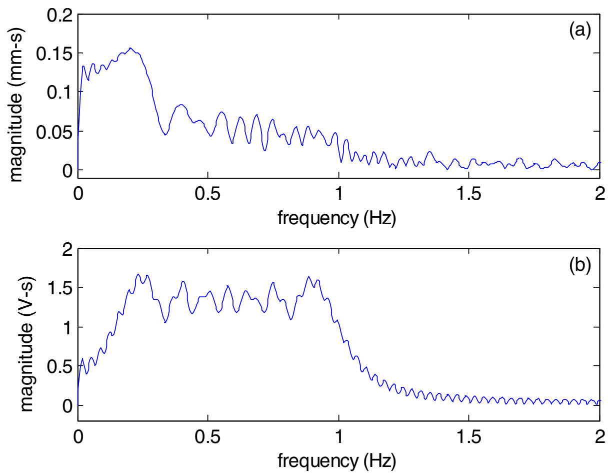

Figure 5. (a) FFT magnitude of the measured displacement. (b) FFT magnitude of the chirp input signal.

3. System identification

In this section, a dynamic model of the EAP actuator by system identification is presented. The persistency of excitation is guaranteed by selecting the reference input signal to have a desired range of frequency with sufficient amplitude [17]. A low-voltage signal (0.1–7.0 V) was applied across the thickness of the EAP strip, and the bending of the EAP strip was recorded with the laser displacement sensor. The largest deflection could be obtained at the resonant frequency of the EAP strip.

3.1. Response to a chirp-signal input

Although other arbitrary waveforms can be applied to generate desired motion, the chirp signal response offers the control of both amplitude and frequency range of the input [18]. The dwelling time and the frequency interval are keys to control the degree of dynamic equilibrium [19].

Figure 4(a) shows such a chirp-signal response of our EAP-strip actuator. The chirp signal input shown in figure 4(b) excited the actuator in the interesting frequency range of (0.01 Hz, 1 Hz) for 30 s at a sampling frequency of 250 Hz. The chirp-signal testing is particularly appropriate for nonlinear systems because the analysis of the test results is usually easier for sinusoidal excitation than others [19]. The frequency of a chirp signal such as shown in figure 4(b) is strictly controlled to be within the range between the starting (0.01 Hz) and ending (1 Hz) frequencies.

Figure 5(a) is a fast Fourier transform (FFT) of the output displacement shown in figure 4(a). The FFT magnitude in figure 5(a) decreases with respect to the increasing frequency due to the band-limited dynamics of the EAP actuator. Figure 5(b) shows an FFT magnitude of the chirp signal input shown in figure 4(b). Since the amplitude of the chirp signal input is constant, its FFT magnitude from 0.01 to 1 Hz looks like a flat hat.

3.2. Developing an ARMAX model

There are many ways to represent the system model, but we used a common ARMAX method based on the best fit of the input–output data. For the system identification the discrete-time model structure for the EAP actuator was set as follows:

$$A(q)y(t) = B(q)u(t) + C(q)e(t), \tag{1}$$

where y is the measured output, u is the manipulated or exogenous input sequence, and e is the white noise [20, 21]. The polynomials $A(q)$, $B(q)$, and $C(q)$ in the shift operator q were found to be

$$\begin{aligned} A(q) &= 1 - 1.995\,q^{-1} - 1.034q^{-2} - 0.038\,81q^{-3} \\ B(q) &= 0.0204 - 0.037\,32q^{-1} - 0.017q^{-2} \\ C(q) &= 1 - 1.487q^{-1} + 0.5119q^{-2} - 0.069\,48q^{-3}. \end{aligned} \tag{2}$$

The coefficients of the polynomials $A(q)$, $B(q)$, and $C(q)$ are identified by minimizing a prediction error. The Matlab command 'armax' was extensively used to design the parametric model structure since it may be necessary to define the model structure that is not a black-box type, but contains a more detailed internal structure reflecting some physical insights regarding how the system behaves. From (1), we found the transfer function $P(z)$ between the input and the output which represents the dynamics of the system:

$$P(z) = \frac{0.027\,52z^3 - 0.051\,63z^2 + 0.0242z}{z^3 - 0.9644z^2 - 0.9194z + 0.8845}. \tag{3}$$

We had applied several system-identification methods such as autoregression (AR), autoregression with exogeneous input (ARX), autoregressive moving average with exogeneous input (ARMAX), output-error (OE), and Box–Jenkins (BJ). Among these linear methods and various orders of the model structure, we constructed a third-order ARMAX model structure since it captured the best characteristics of the EAP. The order of this model structure was 3 to represent the linearized model. Since there is no pole at the origin, there is no inherent integrating component in the linearized model.

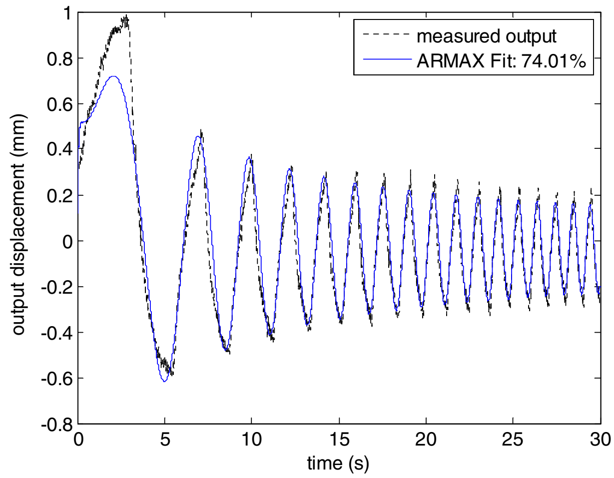

Figure 6. Comparison of the measured output with the ARMAX model's output in response to the chirp signal.

Figure 6 shows the comparison of the experimentally measured actuator output with the ARMAX model's simulated output in response to the same chirp signal. These well-matched responses verify the accuracy of the model. With the good fitting percentage of the experimentally measured output with the simulated linearized model's response, it is reasonable to consider the model linear within this frequency range since the measured output follows the simulated output well. Now, we can design the controller based on the derived system model.

4. Controller design

The control objectives in this research were (1) to have a 60° phase margin, (2) to follow step position commands without a steady-state error, and (3) to minimize the settling time. To achieve these control objectives, a discrete PID controller was designed for the EAP actuator. The discrete PID compensator with bilinear transformation can be written as follows [22]:

$$\frac{\left(K_P + \frac{2K_D}{T_S}\right) z^2 + \left(K_I T_S - \frac{4K_D}{T_S}\right) z + \left(-K_P + K_I T_S + \frac{2K_D}{T_S}\right)}{z^2 - 1}, \tag{4}$$

where T_S, K_P, K_I, and K_D are the sampling period of the discrete-time system, and the proportional, integral, and derivative gains, respectively. The proportional–integral (PI) term is necessary to meet the zero steady-state error requirement. The proportional–derivative (PD) term is used to reduce the overshoot. The PI and PD corner frequencies were calculated with a pole-zero cancellation method. The parameter values were calculated from the comparison of (4) with a second-order transfer function (5).

$$C(z) = k_c \frac{(z - p_{d1})(z - p_{d2})}{z^2 - 1}, \tag{5}$$

where k_c is calculated to set the 60° phase margin with a crossover frequency of 0.171 Hz in the loop transfer function, and p_{d1} and p_{d2} are discrete poles of the plant model. If poles are close to the origin, the system response will be slower. Therefore, canceling the poles close to the origin will enhance the tracking performance. The values of the matching parameters of the controller from (4) and (5) are given in table 2.

Table 2. List of parameter values used for experiments.

$T_S = 0.004$ s	$p_{d1} = -0.9583$
$K_P = 0.648\,94$ V mm^{-1}	$p_{d2} = 0.9279$
$K_I = 11.688\,17$ V mm^{-1} s^{-1}	$K_a = 0$ mm V^{-1} (without the anti-windup scheme)
$K_D = 0.000\,03$ V s mm^{-1}	$K_a = 50$ mm V^{-1} (with the anti-windup scheme)
$k_c = 0.662\,25$ V mm^{-1}	

Table 3. Summary of simulated time-domain transient responses.

	Overshoot M_p (%)	Settling time t_s (s)	Rise time t_r (s)
Without saturation block	10.33	6.26	1.35
With saturation block	3.24	13.29	1.69
With anti-windup block	1.58	4.61	1.69

Figure 7 shows a Simulink Real-Time Workshop schematic diagram for the closed-loop digital position control of the EAP actuator with an integrator anti-windup scheme. The controller includes an anti-windup term which reduces the degradation in the system performance due to actuator saturation.

The anti-windup gain K_a needs to be large enough so that the anti-windup scheme can keep the control effort to the integrator small [22]. The purpose of the saturation block, in the Simulink block diagram is to prevent an excessive control voltage from being applied to the EAP actuator. The control voltage was limited to ±7 V to avoid permanently damaging the EAP strip.

5. Simulation and experimental results

5.1. Simulated 0.8 mm step response

Simulation results of the EAP actuator's closed-loop tracking performance are presented in figure 8. The dotted line from figure 8(a) indicates the system response without the saturation block, and figure 8(b) shows how much the control voltage was applied to the system. Dash–dotted lines demonstrate the effect of the saturation in the step response. The simulation result with the full controller including the anti-windup scheme is shown with a solid line. Therefore, the effectiveness to limit the actuator saturation with this anti-windup scheme could be anticipated from these simulation results.

The accomplished time-domain transient responses in figure 8 are summarized in table 3. The settling time was calculated within 5% of the steady-state value and the rise time was calculated for the response time from 10% to 90% of the steady-state value. The overshoot (M_p) decreased to 1.58% from 3.24%, and the 2% setting time (t_s) also decreased to 4.61 s from 13.29 s. As we expected with using the anti-windup scheme, the control system with anti-windup exhibited substantially less overshoot and settling time.

5.2. Experimental 0.8 mm step response

Figure 9 shows a 0.8 mm closed-loop position response of the EAP actuator demonstrating the effectiveness of the

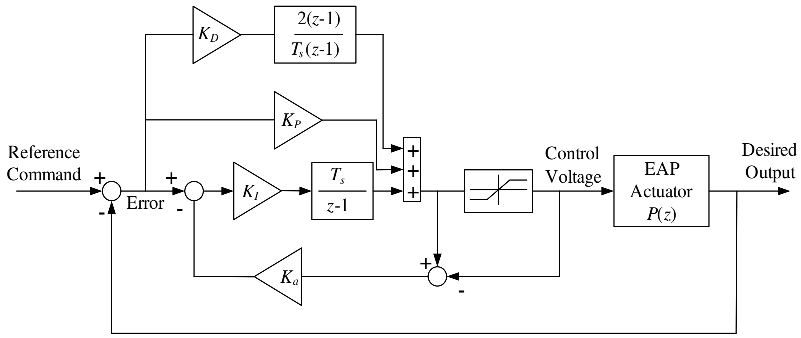

Figure 7. Schematic diagram of the closed-loop position control of the EAP actuator.

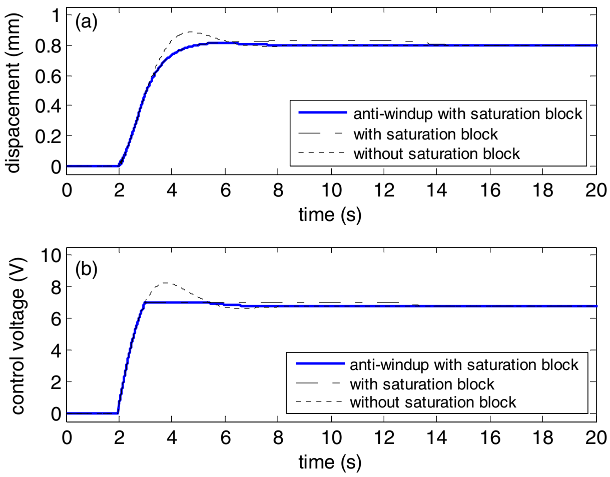

Figure 8. (a) Simulated closed-loop step response to a 0.8 mm step command using the digital PID controller (4) without (dotted) and with (dash–dotted) the saturation block, and with the anti-windup scheme along with the saturation block (solid). (b) Corresponding control voltages applied to the plant.

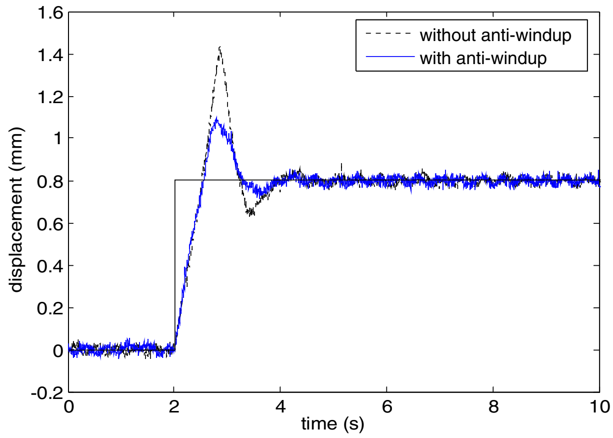

Figure 9. Experimental tracking performances of a 0.8 mm step command using the digital PID controller with and without the anti-windup scheme.

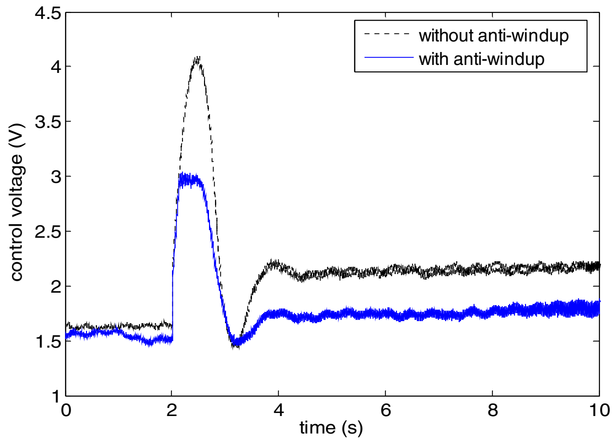

Figure 10. Control voltage profiles with and without the anti-windup scheme.

Table 4. Summary of experimental time-domain transient responses.

	With the anti-windup scheme	Without the anti-windup scheme
Overshoot (M_p)	37.1%	79.7%
Settling time (t_s)	1.61 s	1.79 s
Peak time (t_p)	0.79 s	0.87 s

anti-windup scheme very well. For precision position control, the anti-windup scheme helped to reduce the overshoot and the control voltage only when the actuator was saturated. The steady-state error was also eliminated. This is very important to manipulate the micro-actuator effectively in 'pick-and-place' operations. The accomplished time-domain transient responses in figure 9 are summarized in table 4.

With the implemented anti-windup scheme, the peak control voltage decreased by 25.7% and the overall control voltage decreased by 16.1% as shown in figure 10. Note that the spike in the control voltage is caused by the accumulated error due to actuator saturation. Since the laser displacement sensor's conversion factor is 1 mm per 1 V, the difference in the two initial control voltage profiles in figure 10 indicates the difference in the initial sensor readings of the tip position of EAP strip. Each time the EAP actuator's initial reference position is set, the value of the control voltage might be slightly different since the EAP actuator is manually adjusted somewhere in the sensing range of the laser displacement

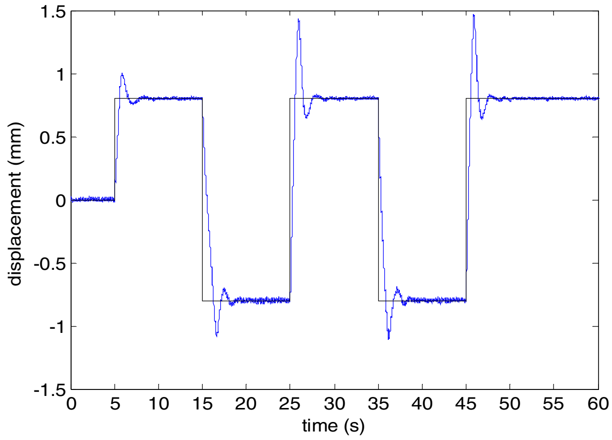

Figure 11. The tracking performance of a series of 0.8 mm back-and-forth step commands using the digital PID controller with the anti-windup scheme.

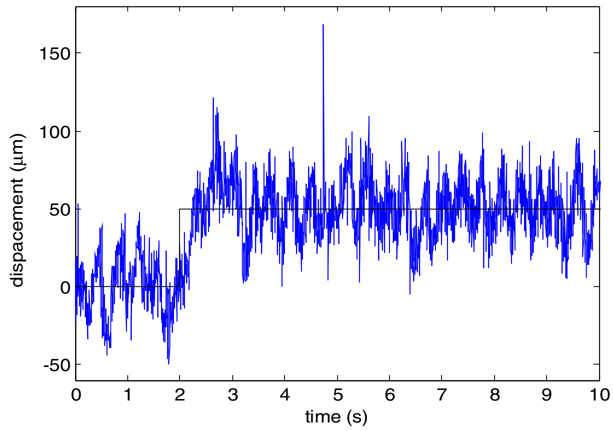

Figure 13. 50 μm closed-loop step response of the EAP actuator.

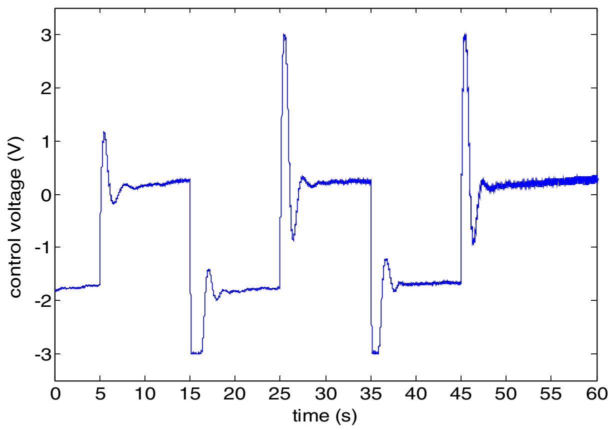

Figure 12. Control voltage profiles with the anti-windup scheme for the 0.8 mm back-and-forth step commands.

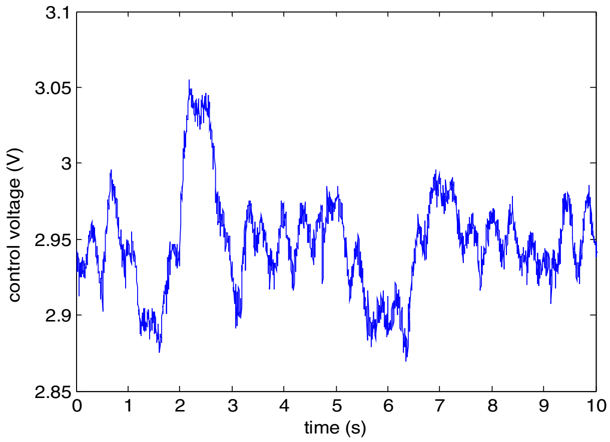

Figure 14. Control voltage profile of the 50 μm closed-loop step response of the EAP actuator.

sensor. Therefore, as shown in figure 10, the non-zero initial control voltage was required to regulate the zero reference position of the EAP actuator.

After the 0.8 mm step was made, the whole closed-loop control system must maintain a larger EAP defection. Thus the control signal actually increased. As shown in figure 10, the steady-state control input without the anti-windup scheme (dashed line) was about 2.2 V. After the anti-windup scheme was applied, it was reduced to 1.8 V. This reduction in the control voltage also demonstrates the effectiveness of our anti-windup scheme.

5.3. Experimental back-and-forth step response

The main reason for using the anti-windup scheme is to improve the transient performance when the controller is saturated. If there were a constant offset between the desired output and the actual output, the anti-windup scheme would not work properly. The output swing of the actuator output should be sufficient, otherwise the actuator should be replaced because of its limitation. An additional experimental result with a series of 0.8 mm back-and-forth step commands was performed every 10 s and presented in figure 11. The first +0.8 mm step command was applied at 5 s without the saturation. However, the saturation occurred at 15 and 35 s since the control voltage was limited by ± 3 V, which is prominent in figure 12. The reason for different overshoots between 5 and 25 s or 45 s might be the different step commands applied since the first step command was zero to +0.8 mm. However, the third or the fifth step command was -0.8 to +0.8 mm, so a larger control voltage needed to be generated by the controller.

5.4. Microscale position control

The EAP actuator has significant potential to be used as a micro- or nano-manipulation device. Figures 13 and 14 show a 50 μm closed-loop step response and the corresponding control voltage. Since the control input is well within the operation range of ± 7 V, no integrator wind-up took place, and the difference between the minimum and the maximum control voltage was only 0.186 V in figure 14.

In figure 13, conspicuous fluctuations in the position data are present. The control voltage shown in figure 14 also fluctuates to attempt to compensate for these position

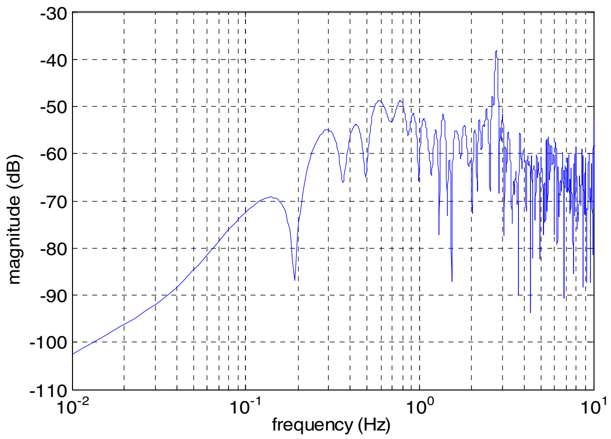

Figure 15. FFT analysis of the 50 μm step response of the EAP actuator.

fluctuations. A 50 μm step input was applied on the EAP actuator at 2 s. The control voltage shown in figure 14 indicates the increased control effort at this time. After 2 s, the EAP actuator followed the step input with the required control voltage. The measured displacement output and the control effort in the 50 μm step response in the closed-loop system contained significant fluctuation due to the sensor noise as shown in figure 13. Thus, we believe the trough around 6 s is random noise generated by the sensor.

An FFT analysis of the closed-loop step response given in figure 15 shows a strong signal power at approximately 2.8 Hz. This 2.8 Hz vibration component is believed to originate from the first resonance mode of the EAP actuator. Even with this resonance, the position resolution of this EAP actuator is better than 50 μm.

6. Conclusions

In this paper, an EAP actuator's dynamic behavior was discussed, and its system identification and precision control were performed by simulation and experimental implementation. The digital PID controller based on the identified model improved the system performance. The phase margin was 60° with a crossover frequency of 0.171 Hz. The 0.8 mm and 50 μm step responses demonstrated significant improvements in transient dynamic behaviors. The settling time was reduced by 0.18 s, the control voltage was reduced by 16.3%, and the per cent overshoot decreased to 37.1%. Performance degradation due to actuator saturation could also be reduced significantly. The proposed anti-windup scheme along with the controller proved that an excellent tracking performance could be achieved.

Acknowledgments

We are grateful to Drs Othon K Rediniotis and Hyoung-yoll Jun of Texas A&M University for providing us with EAP samples.

References

[1] Sadeghipour M, Salomon R and Neogi S 1992 Development of a novel electrochemically active membrane and 'smart' material based vibration sensor/damper *Smart Mater. Struct.* **1** 172–9
[2] Shahinpoor M 1992 Conceptual design, kinematics and dynamics of swimming robotic structures using ionic polymer gel muscles *Smart Mater. Struct.* **1** 91–4
[3] Oguru K, Kawami Y and Takenaka H 1992 Bending of an ion-conducing polymer film–electrode composite by an electric stimulus at low voltage *J. Micromachine Soc.* **5** 27–30
[4] Tadokoro S, Yamagami S, Takamori T and Oguro K 2000 Modeling of nafion–Pt composite actuators (ICPF) by ionic motion *Proc. SPIE Smart Struct. Mater.* **3987** 92–102
[5] Bar-Cohen Y, Sherrit S and Lih S 2001 Characterization of the electromechanical properties of EAP materials *Proc. SPIE's 8th Annual Symp. on Smart Structures and Materials* (Bellingham, WA: SPIE Optical Engineering Press) pp 4326–43
[6] Kanno R, Tadokoro S, Hattori M, Takamori T, Costaftis M and Oguro K 1995 Dynamic model of ICPF (ionic conducting polymer film) actuator *Proc. IEEE Int. Conf. on Systems Man, and Cybernetics: Intelligent Systems for the 21st Century* vol 1 (Piscataway, NJ: IEEE) pp 177–82
[7] Kanno R, Tadokoro S, Hattori M, Takamori T, Costaftis M and Oguro K 1995 Modeling of ICPF (ionic conducting polymer film) actuator *Proc. 1995 IEEE 21st Int. Conf. on Industrial Electronics, Control, and Instrumentation* vol 2 (Piscataway, NJ: IEEE) pp 913–18
[8] Kanno R, Tadokoro S and Takamori T 1996 Linear approximate dynamic model of ICPF *Proc. IEEE Int. Conf. on Robotics and Automation* vol 1 (Piscataway, NJ: IEEE) pp 219–25
[9] Bhat N and Kim W J 2004 Precision force and position control of ionic polymer metal composite *J. Syst. Control Eng.* **6** 421–32
[10] Bhat N 2003 Modeling and precision control of ionic polymer metal composite *Master's Thesis* Texas A&M University
[11] Newbury K and Leo D J 2002 Modeling of electromechanical transduction in ionic polymer materials *Proc. ASME Int. Mechanical Engineering Congr. & Exposition (New Orleans, LA)* (ASME) pp 47–57
[12] Alvarez R J and Shahinpoor M 2002 Simulation and control of iono-elastic beam dynamic deflection model *Proc. SPIE Smart Struct. Mater.* **4695** 335–44
[13] *Biomimetic Products Datasheet* (Sterling, VA: Biomimetic Products Inc.)
[14] Mallavarapu K and Leo D J 2001 Feedback control of the bending response of ionic polymer actuators *J. Intell. Mater. Syst. Struct.* **12** 143–55
[15] Richardson R C, Levesley M C, Brown M D, Hawkes J A, Watterson K and Walker P G 2003 Control of ionic polymer metal composites *IEEE/ASME Trans. Mechatron.* **8** 245–53
[16] Shahinpoor M and Kim K J 2001 Ionic polymer–metal composite: I. Fundamentals *Smart Mater. Struct.* **10** 819–33
[17] Tao G and Ioannou P A 1988 Persistency of excitation and overparameterization in model reference adaptive control *Proc. 27th Conf. on Decision and Control (Austin, TX)* (IEEE) pp 757–58
[18] Ewins D 1986 *Modal Testing: Theory and Practice* (Nærum Denmark: Brüel and Kjær)
[19] Harris C 1995 *Shock and Vibration Handbook* (New York: McGraw-Hill)
[20] Ljung L 1999 *System Identification Theory for the User* (Upper Saddle River, NJ: Prentice-Hall)
[21] Soderstrom T and Stoica P 1989 *System Identification* (Upper Saddle River, NJ: Prentice-Hall)
[22] Franklin G F, Powell J D and Emami-Naeini A 2002 Feedback *Control of Dynamic Systems* 4th edn (Upper Saddle River, NJ: Prentice-Hall)